AIAA SciTech Forum
January 3-7, 2022, San Diego, CA & Virtual
AIAA SCITECH 2022 Forum

10.2514/6.2022-1615

Aero-Thermo-Elastic Optimization Using the Discrete Adjoint Approach

Soudeh Kamali[1], Dimitri J. Mavriplis[2]
Department of Mechanical Engineering, University of Wyoming, Laramie, WY, 82070, USA

Evan M. Anderson[3]
Department of Wing Energy, Sandia National Laboratories, Albuquerque, NM, 87185, USA

Coupled aero-thermal-elastic sensitivity analysis and optimization is required for accurate design and optimization in many high-speed flow problems. Hence, the multidisciplinary optimization of such problems is the main focus of the current work. In this study, the flow simulations are carried out using NSU3D, a three-dimensional implicit finite volume solver developed in-house. NSU3D's flow and sensitivity analysis capabilities have been well tested through numerous previous studies. For the thermal and structural solutions, a finite-element solver called AStrO is used, which is also developed in-house. AStrO's thermo-elastic analysis and sensitivity analysis capabilities have been demonstrated in previous work as well. In earlier papers we have developed and validated an aero-thermo-elastic analysis platform by coupling NSU3D and AStrO. The purpose of the current work is to demonstrate aero-thermo-elastic optimization by coupling the sensitivities from these two solvers. In this paper, the coupled sensitivities are verified and used in the multidisciplinary optimization of a heated panel in hypersonic flow.

I. Nomenclature

L	=	objective function
D	=	design variables
u_F	=	state variables from the fluid discipline
u_S	=	state variables from the structure discipline
u_T	=	state variables from the thermal discipline
R_F	=	residual from the fluid discipline
R_S	=	residual from the structure discipline
R_T	=	residual from the thermal discipline
Λ_F	=	adjoint from the fluid discipline
Λ_S	=	adjoint from the structure discipline
Λ_T	=	adjoint from the thermal discipline
Ω	=	spatial domain of integration
R	=	residual
C	=	viscous damping matrix
M	=	mass matrix
K	=	stiffness matrix
T	=	temperature
Q	=	volumetric heat source
k	=	thermal conductivity
C	=	specific heat capacity
α	=	thermal expansion

[1] PhD Student, Department of Mechanical Engineering, AIAA Member.
[2] Professor, Department of Mechanical Engineering, AIAA Associate Fellow.
[3] PhD, Department of Wind Energy Technologies Sandia National Laboratories.

E = Modulus of elasticity
v = Poisson's ratio
ρ = density
t = time
l = length of the geometry
u = displacement vector in a structure
$\dot{u}$ = velocity vector in a structure
$\ddot{u}$ = acceleration vector in a structure
T_0 = initial temperature
u_i = vector displacement of a point in a structure
$\dot{u}_i$ = vector velocity of a point in a structure
$\ddot{u}_i$ = vector acceleration of a point in a structure
t_i = traction applied over the surface of a structure in vector form
ξ = damping coefficient
σ_i = stress at a point in a structure in vector form
ϵ_i = strain at a point in a structure in vector form
C_{ijkl} = elastic stiffness tensor
f_i = body force per unit volume at a point in a structure in vector form
N_{ij} = shape functions

II. Introduction

Most practical engineering problems involve interactions between various disciplines. Therefore, the computational design of such problems, must account for the coupling between the different disciplines. This coupling allows for each model to provide complementary information to the other, and therefore, eliminates many assumptions. An optimum multidisciplinary design is only reached after cycling between the different disciplines involved [1]. An important example of this type of problem is fluid-structure interaction. In recent years, the development of supercomputers has made simulation of coupled fluid-structure interactions possible. However, in many engineering designs it is not sufficient to just take into account the interaction of the fluid forces and structural deformations; temperature plays an important role as well [2, 3]. Hypersonic vehicles, for example, go through a wide range of flow conditions with large gradients of velocity and temperature close to their surface [4]. One of the major design concerns at these hypersonic velocities is the high rates of heat transfer experienced by the vehicle [5]. Therefore, it is essential to account for the effect of temperature in order to obtain accurate numerical designs [6, 7].

The success of a high-speed aircraft design relies on the precise calculation of all the following: Aerodynamic loads (aerodynamic pressure and viscous forces), aero-thermal effects (surface heating rate and inner temperature distributions), and structural loads (structural deformation and stresses) [1, 8, 9]. Since the overall performance of an aeronautical system is governed in many cases by these coupling effects, the study of aero-thermo-elastic analysis and optimization methods are of great importance [10]. Recently, a significant amount of work has appeared focusing on aero-thermal, aero-elastic, and aero-thermo-elastic codes for hypersonic flows [4, 11-19]. However, more study is needed to understand all of the physics involved and to refine high-fidelity aero-thermo-elastic analysis and design.

There are two main approaches to solving optimization problems: gradient-based and global search methods [20]. Gradient-based optimization methods are more popular within the field of aerodynamics. This is because of the lower number of analysis runs or function evaluation required for these methods in comparison to the global search techniques [21]. Gradient-based optimizations require the gradients of the objective function and constraints with respect to the design variables. These gradients are referred to as the sensitivity derivatives [22].

The finite-difference method is one of the simplest methods for computing the sensitivity derivatives. Although this approach is easy to implement, it is not the most efficient method. One problem with this approach is that it is computationally expensive, which makes it unsuitable for complex cases with many design variables [23]. Another problem is that the choice of the step size affects the accuracy of the gradient approximation [22]. Therefore, it is better to calculate the sensitivities analytically. When calculating the sensitivity derivatives with the analytical approach, an additional level of simulation referred to as the sensitivity analysis, is required [22]. For sensitivity analysis a choice has to be made between the direct/tangent method and the adjoint method.

The adjoint approach has the advantage of computing cost-function gradients at a cost independent of the number of design variables [23]. This characteristic makes the adjoint method extremely efficient for high-fidelity,

multidisciplinary design problems [24-27]. For such problems, the discrete adjoint is highly favored since it follows the discretization of the governing equations naturally and enables a methodical approach for obtaining the sensitivities for any arbitrarily complex analysis procedure [21, 28, 29].

In this work we study the optimization of aero-thermo-elastic problems using the flow solver and structural solver developed in-house. For this purpose, we use the aero-thermo-elastic analysis platform developed and validated in reference [11]. The premise of the current work is that a modern aero-thermo-elastic design optimization must include high-fidelity models for all the disciplines involved.

This paper is structured as follows. Section III gives details on the aero-thermo-elastic coupling platform by taking a look at each of the required components and the governing equations of each discipline. Section IV briefly presents the equations that are used to obtain the aero-thermo-elastic sensitivities employed in this study. In section V we take into account the aero-thermo-elastic simulation of a heated panel case. This case is used to verify the coupled thermo-elastic and aero-thermo-elastic sensitivities. The verified adjoint sensitivities are then used in the aero-thermo-elastic optimization of the panel in hypersonic flow. Section VI draws conclusions and highlights future work.

III. Aero-Thermo-Elastic Coupling

Generally, when approaching a multidisciplinary simulation, there are two options available: strong and weak coupling. In the first case, the flow, elasticity and heat transfer equations are treated as one single system of equations and solved at once using a single numerical framework. In the second case, the solution of each discipline is obtained from independent codes and then coupled together by exchanging boundary conditions at the interface between the domains [30, 31]. It is easier to achieve stability for the strong coupling approach; however, it suffers from the inability to use already available and well-tested solvers. On the other hand, the weak coupling approach is able to use existing, well-developed and tested codes for each discipline. This approach does however have its own disadvantages. These are: the problem of stability and the difficulty of transferring data between the individual disciplinary codes [32, 33].

The code-coupling can be very challenging in practice. The two main challenges, which arise from the discontinuities between the models, are: time-scale discontinuity, and space-scale discontinuity [7, 34]. In the following pages we explain how we dealt with each of these challenges in developing our in-house aero-thermo-elastic analysis platform. A detailed description of the aero-thermo-elastic analysis platform is given in references [11, 18, 19]. This platform couples the three disciplines through a weak coupling approach. This decision was made to allow us to take advantage of the already available and tested high-fidelity flow solver and structural solver developed in-house for multidisciplinary modeling and optimization.

In the rest of this section, we briefly look at the different components of the numerical set up required to run an aero-thermo-elastic simulation: the flow solver, the structural solver (elasticity and thermal equation), fluid-structure interaction (FSI) module, and the mesh deformation capability.

A. Flow Solver

The flow solver used in this study is the "Navier-Stokes Unstructured 3D" (NSU3D) code, which is a Reynolds-averaged Navier-Stokes (RANS) solver for unstructured grids [24]. It is a vertex-centered finite volume solver, which is second-order accurate in both time and space. This flow solver uses a line-implicit agglomeration multigrid algorithm, which can be used either as a non-linear solver, or a linear solver within an approximate Newton method, or as a pre-conditioner for GMRES for driving the non-linear steady-state residual to zero [35]. For time-dependent problems, all the above-mentioned solvers can be used in a dual-time stepping approach for solving the non-linear problem, which arises at each time step [36]. NSU3D has been widely validated for both steady-state and time-dependent flow problems, having been used in numerous simulations and participations in events such as the Drag Prediction Workshop, the High-Lift Prediction Workshop, and the Aero-elastic Prediction Workshop series [37-40]. In recent years, NSU3D has been extended for use in coupled aero-elastic, aero-thermal, and aero-thermo-elastic calculations [11, 18, 19, 21, 36, 41]. Detailed explanation of this solver can be found in previously available references [24, 42, 43]. As such, only a concise description of the formulations is given in this paper.

The flow solver is based on the conservative form of the Navier-Stokes equations. These may be written as:

$$\frac{\partial u(x,t)}{\partial t} + \nabla . F(u) = 0 \tag{1}$$

For moving mesh problems, the above formulation is written in arbitrary Lagrangian-Eulerian (ALE) form, as:

$$\frac{\partial Vu}{\partial t} + \int_{B(t)} [F(u) - \dot{x}u] . ndB = 0 \tag{2}$$

here V refers to the volume of the control volume bounded by a control surface $B(t)$, $\dot{\mathbf{x}}$ is the vector of mesh face or edge velocities, and n is the unit normal of the face or edge. Vector u denotes the state vector of conserved variables, and the flux vector F contains both inviscid and viscous fluxes. The equations are closed with the perfect gas equation of state for all cases presented in this work [21, 42].

The time derivative term is discretized using a second-order accurate backward difference formula (BDF2) scheme, leading to the implicit system of equations at each time step given as:

$$\frac{3}{2\Delta t}V^n u^n - \frac{2}{\Delta t}V^{n-1}u^{n-1} + \frac{1}{2\Delta t}V^{n-2}u^{n-2} + S^n(u^n, x^n, \dot{x}^n) = 0 \tag{3}$$

where $V^n = V(x^n)$ represents the mesh control volumes and $S^n(u^n, x^n, \dot{x}^n)$ represents the spatial discretization terms at the n^{th} time step.

The functional dependence of the implicit system to be solved at each time step can be written in residual form as:

$$R^n(u^n, u^{n-1}, u^{n-2}, x^n, x^{n-1}, x^{n-2}) = 0, \quad n = ,2,3, \dots, N \tag{4}$$

where the initial conditions are given by u^0 and x^0, and noting that a BDF1 time discretization is used for the first time step.

At each time step, the implicit residual is solved using a line-implicit solver with agglomeration multigrid. For all the cases presented in this work, the fluxes are calculated using the Roe scheme [44]. It should also be mentioned that that the flow medium is considered as perfect gas in the numerical simulations.

Considerable effort has been spent in previous work for implementing and verifying the discrete adjoint approach for computing sensitivities within the NSU3D unstructured mesh RANS CFD solver. Exact sensitivities can be calculated for both steady-state and time-dependent problems in the NSU3D framework using the adjoint and tangent methods [36, 43, 45].

B. Structural Solver

The structural solver used in this study is a finite-element solver named AStrO (Adjoint-based Structural Optimizer), which was developed in-house. AStrO has been introduced in previous work [11, 12, 21, 36, 41, 46] and supports both linear and nonlinear finite-element modeling of three-dimensional structures [41]. AStrO also supports finite-element modeling of the thermo-elastic behavior of structures. AStrO can run static or dynamic analysis of either the heat transfer problem, or the elasticity problem, or the two coupled disciplines [46]. The motivation for constructing an in-house structural solver was to enable tight coupling as well as for calculating sensitivities for coupled CFD and Computational Thermal and Structural Dynamics (CTSD) problems using adjoint methods [21] .

AStrO is compatible with existing commercial structural analysis software tools such as Abaqus [47]. It contains an interface that can process model input files generated by Abaqus [36]. Dynamic systems are modeled with implicit second-order accurate time integration by the Hilber-Hughes-Taylor "alpha" method [48]. The discretized equations for the elasticity problem are derived from the widely used virtual work formulation [48]. The temperature distribution due to heat conduction through a structure is governed by the Poisson equation, which is discretized in a similar manner as the equations of elasticity. In the following paragraphs we take a closer look at AStrO's governing equations.

The transient elasticity equation solved in AStrO is given as:

$$\nabla \cdot \sigma - \xi \frac{du}{dt} - \rho \frac{d^2u}{dt^2} + f = 0 \tag{5}$$

where f represents the applied body forces, u is the vector of displacements, σ is the stress tensor, and ξ is the damping coefficient.

The principle of virtual work [49] applied to the equations of elasticity discretized using the finite element method yields:

$$\int_\Omega \sigma_i \frac{\partial \epsilon_i}{\partial U_j} d\Omega + \int_\Omega \xi \dot{u}_i N_{ij} d\Omega + \int_\Omega \rho \ddot{u}_i N_{ij} d\Omega - \int_\Omega f_i N_{ij} d\Omega - \int_S t_i N_{ij} dS = 0 \tag{6}$$

where N_{ij} is a matrix of basis functions and U_j is a vector of nodal solution parameters, or degrees of freedom. $\dot{u}_i$ and $\ddot{u}_i$ are the velocity and acceleration vectors at a point in the structure, σ and ϵ are the stress and strain, ξ is the damping

coefficient, ρ is the mass density, f_i is the applied body force per unit volume, and t_i is the applied surface traction per unit area on the structure. The final term is the integral of traction over the surface area of the structure, while all other terms are volume integrals over the body of the structure [41, 46]. The matrix equivalent of Eq. (6) can be reduced to the system of equations:

$$[K]\,U + [C]\,\dot{U} + [M]\,\ddot{U} = F \tag{7}$$

where $[K]$ is the stiffness matrix, $[M]$ is the mass matrix, $[C]$ is the viscous damping matrix, F is the vector of forces, U is the vector of nodal values displacements, $\dot{U}$ vector of nodal values of velocities, and $\ddot{U}$ vector of nodal values of acceleration.

The transient heat equation solved in AStrO is given as:

$$\rho c \frac{\partial T}{\partial t} + \nabla \cdot (k \nabla T) - Q = 0 \tag{8}$$

where, Q is the rate of internal heat generation per unit volume, k is the thermal conductivity, c is the specific heat capacity, ρ the density, and T is the temperature.

The discretized governing equations for heat conduction in structures derived from the variational form using the finite element method is:

$$-\int_\Omega \; q_i \frac{\partial N_j}{\partial x_i} d\Omega + \int_\Omega \; \rho C_p \dot{T} N_j d\Omega - \int_\Omega \; Q N_j d\Omega + \int_S \; q_i n_i N_j dS = 0 \tag{9}$$

where n_i is the normal vector, q_i is the surface heat flux, and N_j the basis function. The matrix equivalent is then obtained as shown in Eq. (10):

$$[K_{therm}]\,T + \; [M_{therm}]\,\dot{T} = F_{therm} \tag{10}$$

where the vector T represents nodal values of temperature, $[K_{therm}]$ is the global thermal conductivity matrix, $[M_{therm}]$ is the thermal mass matrix, and F_{therm} is the vector of internal heat generation sources.

AStrO is capable of modeling the coupled thermo-elastic responses in structures. However, there are several simplifying assumptions made. The first assumption is that thermal material properties such as conductivity and specific heat capacity have no significant dependence on strain. Furthermore, the heat generated by deformation is assumed to be negligible. In other words, the deformation has a one-way dependence on the temperature distribution. These assumptions are acceptable, since the cases to be considered are expected to have small values of strain and within the elastic regime, selected materials will have low internal damping characteristics, and deformation rates will not produce significant heat through phenomena such as viscoelasticity [46].

Under these assumptions, in any given analysis, the temperature distribution of a structure can be obtained first, followed by the deformation solution based on the temperature results in addition to applied loads. To account for the dependence of deformation on the temperature distribution, an adjustment to the definition of total strain is required. Any point in the structure that is subject to a combination of applied stress and change in temperature will exhibit a measure of strain for each of those contributors. Hence, the total strain can be expressed as:

$$\epsilon_k^{total} = \epsilon_k^{stress} + \epsilon_k^{therm} \tag{11}$$

In the governing equations of elasticity based on the principle of virtual work, stress at a point under the assumption of linear elasticity can be expressed as:

$$\sigma_i = C_{ik}\epsilon_k \tag{12}$$

Fundamentals of continuum equilibrium mandate that the stress and strain matrices be symmetric, so that $\sigma_{ij} = \sigma_{ji}$ and $\epsilon_{kl} = \epsilon_{lk}$. Therefore, here they have been expressed more concisely as one-dimensional vectors, adopting a single subscript index for normal stresses and strains. In Eq. (12), C_{ik} is the stiffness matrix of the local material. However, ϵ_k must only be the strain due to the applied stress. Therefore, in the presence of thermal expansions, we have:

$$\sigma_i = C_{ik}\epsilon_k^{stress} = C_{ik}\left(\epsilon_k^{total} - \epsilon_k^{therm}\right) \tag{13}$$

The strain due to thermal expansion is assumed to be linearly related to temperature, such that the change in temperature from some reference temperature T^{ref} multiplied by a vector of thermal expansion coefficients α gives the resulting thermal strain to be:

$$\epsilon_k^{therm} = (T - T^{ref})\alpha_k = \Delta T \alpha_k \tag{14}$$

Then the governing equations for the elastic response taking into account the change in temperature, becomes:

$$\int_\Omega C_{ik}\left(\epsilon_k^{total} - \Delta T \alpha_k\right)\frac{\partial \epsilon_i}{\partial U_j} d\Omega + \int_\Omega \xi \dot{u}_i N_{ij} d\Omega + \int_\Omega \rho \ddot{u}_i N_{ij} d\Omega - \int_\Omega f_i N_{ij} d\Omega - \int_S t_i N_{ij} dS = 0 \tag{15}$$

Separating out the contribution of the thermal expansion from the stress term gives:

$$\int_\Omega C_{ik}\epsilon_k^{total}\frac{\partial \epsilon_i}{\partial U_j} d\Omega + \int_\Omega \xi \dot{u}_i N_{ij} d\Omega + \int_\Omega \rho \ddot{u}_i N_{ij} d\Omega - \int_\Omega f_i N_{ij} d\Omega - \int_S t_i N_{ij} dS - \int_\Omega C_{ik}\Delta T \alpha_k \frac{\partial \epsilon_i}{\partial U_j} d\Omega = 0 \tag{16}$$

Since the temperature solution is pre-computed, the effect of thermal expansion shows up as part of the load in the elasticity equations (or the final three terms in Eq. (16) above). Equation 16 is the augmented form of the governing equations for thermoelastic modeling. AStrO's thermal and thermo-elastic analysis capabilities have been validated in references [46] and [11].

AStrO has the capability of calculating exact sensitivities using the adjoint method [12, 19, 41, 46]. AStrO also offers an on-board optimizer using the steepest-descent line search algorithm with backtracking [50]. This function is convenient for simple problems and for trouble shooting, since it does not require linking with external packages. Alternatively, more sophisticated optimizers can be linked to AStrO for more complex optimization problems [46].

C. Fluid-Structure Interaction (FSI)

Proper data transfer between different disciplines is one of the most important factors in multidisciplinary analysis and design. Correct modeling of aero-thermo-elastic problems requires an accurate coupling of the fluid and structure codes. Although, in these problems the geometry is shared, the models most often have dissimilar meshes. Moreover, boundary data from one domain must be made available on the other domain [51]. The weak coupling method uses an iterative approach to converge the temperature and heat flux distributions at the boundaries of the fluid and structure domains. The computation alternates between the fluid and structure domains with exchange of the above-mentioned boundary conditions [52, 53]. In weakly coupled codes, the CFD and CTSD codes are alternatively called from a master program. This master program is also in charge of transferring data between the codes on the CFD/CTSD interface.

In order to control the stability and convergence in these problems, the choice of the boundary condition is very important. In the literature, the continuity of temperature and heat flux at the interface is mainly implemented by imposing the wall temperature distribution computed from the CTSD solution on the fluid side and the heat flux distribution computed from the CFD solution on the structure side. This method is known as the flux forward temperature back (FFTB) method or the Dirichlet-Neumann boundary condition. Many researchers have shown that the use of this type of boundary condition is the key to achieving numerical stability and having robust convergence [52-55].

A Fluid Structure Interface (FSI) module has previously been created in-house and used for aero-elastic analysis and design problems [21, 36]. This model has been used to transfer the aerodynamic forces from the fluid solver to the structure solver, and in return pass the calculated displacements to the fluid surface mesh [36]. This module was updated so that it can also transfer temperature and heat flux between the fluid and structure meshes. When dealing with the aero-thermo-elastic analysis, we need to exchange the aerodynamic forces and heat fluxes from the fluid domain to the structure domain, and in return send the temperatures and displacements from the structure mesh to the fluid mesh. The effects of the temperature on the structure are dealt with internally in the structure code as explained in the previous section. The transfer of information for the aero-thermo-elastic analysis process is summarized in Fig. 1. At each coupling time step a static fluid problem is solved followed by a transient structural and thermal problem. This approach was taken in order to reduce overall computational expense and is justified by the disparity in time scales between the fluid and structural problems [9, 56].

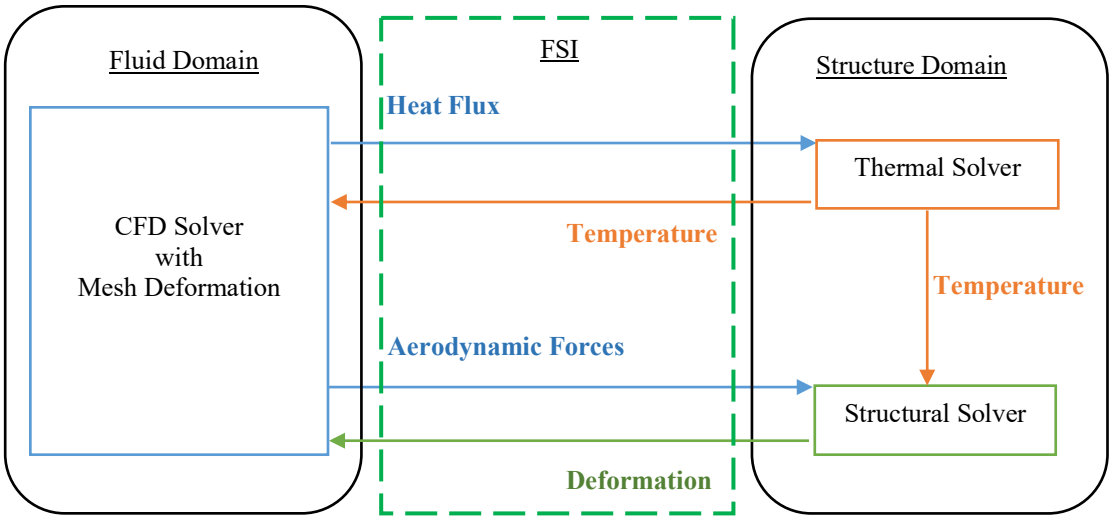

Fig. 1 Transfer of information for the coupled aero-thermo-elastic analysis platform.

In practice the FSI computes the heat fluxes and the aerodynamic forces at each CFD surface mesh point. These values are then projected onto the finite-element basis functions of the structural model where they are assembled in the form of heat fluxes and forces on the finite-element nodal locations. Conversely, once the structural temperature and displacement solutions have been computed, they are transferred back to the surface CFD mesh in a similar manner [21]. This transfer of data between the two meshes can be summarized with the following equations:

$$\begin{cases} Q_{CTSD} = [P]Q_{CFD} \\ T_{CFD} = [P]^T T_{CTSD} \end{cases} \tag{17}$$

$$\begin{cases} F_{CTSD} = [P]F_{CFD} \\ U_{CFD} = [P]^T U_{CTSD} \end{cases} \tag{18}$$

where [P] represents the rectangular transfer matrix which projects pointwise CFD surface heat fluxes and forces onto the individual structure mesh surface points. The transpose of the matrix is used to obtain the CFD surface temperatures and displacements from the structure mesh [36]. The interpolation patterns which define the [P] matrix are computed by locating the perpendicular projection of each point of the surface CFD mesh on the structure model elements [21]. This is done through a fast parallel search technique, which is based on the minimum distance search [57] in order to locate the closest enclosing face on the exposed surface of the structure mesh for each surface point on the fluid mesh. The final transfer corresponds to a piecewise linear interpolation of the aerodynamic loads, heat fluxes, displacements, and temperature between the two meshes. Hence, for conforming surfaces, P corresponds to a matrix of piecewise linear interpolation coefficients.

The in-house developed FSI is capable of working with non-matching fluid and structure meshes with different element types and mesh resolution. Moreover, the developed FSI has the ability to handle fluid and structure models that have non-matching outer-mold line (OML) geometries [36]. Additionally, the FSI formulation is discretely conservative for the transfer of forces and heat fluxes from the fluid to the structure and satisfies the principle of conservation of virtual work for the transfer of displacements from the structure to the fluid domains [58].

D. Mesh Deformation

When dealing with aero-thermo-elastic problems, we require a mesh deformation capability in order to account for the displacements computed by the structural solver in response to the aerodynamic and thermal loads. When running time-dependent problems, we may also have prescribed surface deflections at certain times, such as when simulating prescribed motion of a control surface. Hence, the CFD solver must be modified to take into account the additional dynamics introduced due to the mesh motion, and the fluid equations must be written in the ALE framework [56, 59]. NSU3D employs a discretization that respects the Geometric Conservation Law (GCL) [60] to ensure that the flow solver maintains its accuracy and stability in the presence of arbitrary mesh motion. Significant work has been done

in the past on the development of a robust and efficient mesh deformation technique [61, 62]. This approach is based on the linear elasticity model, and the mesh deformation equations are discretized using a second-order accurate continuous Galerkin finite-element approach [36]. The equations for the mesh deformation are solved using the same line-implicit multigrid algorithm used for solving the flow equations [39].

IV. Aero-Thermo-Elastic Sensitivity Analysis Formulation

In the previous section we have given details of the coupled aero-thermo-elastic analysis platform. NSU3D's flow sensitivity analysis capabilities have been presented in previous work [21, 36, 41, 63]. AStrO's thermo-elastic sensitivity analysis capability has been validated in references [46] and [19]. In this current work, the goal is to perform aero-thermo-elastic optimization using the coupled sensitivities from these two platforms.

In this section, we describe the implementation of the coupled aero-thermo-elastic sensitivities. For the implementation, it is desirable to follow the solution strategies and data structures used for the analysis problem, as closely as possible. This allows the use of the same disciplinary solvers for the respective sensitivity problem. Furthermore, it means that the data transferred between the disciplines consists of vectors of the same dimensions for the analysis, the tangent and adjoint formulations [25, 64]. In the following, the coupled tangent and adjoint formulation are presented. These formulations take into account the specifics of NSU3D, AStrO, and the in-house FSI module.

A. Aero-Thermo-Elastic Tangent Sensitivity Analysis

Starting with the forward sensitivity problem, consider an objective function such as L:

$$L = L(D, u_x(D), u_F(D), u_T(D), u_s(D)) \tag{19}$$

As shown in Eq. (19) above, in addition to an explicit dependence on the design inputs D, there exists an implicit dependence through the state variables u_x, u_F, u_T, u_S, coming from the mesh motion, fluid, thermal, and structure disciplines, respectively. In all the following equations the subscripts x, F , T, and S refer to the mesh motion, fluid, thermal, and structure disciplines respectively. Using the chain rule, the sensitivity of the objective function with respect to the design variables D can be expressed as:

$$\frac{dL}{dD} = \frac{\partial L}{\partial D} + \frac{\partial L}{\partial u_x}\frac{\partial u_x}{\partial D} + \frac{\partial L}{\partial u_F}\frac{\partial u_F}{\partial D} + \frac{\partial L}{\partial u_T}\frac{\partial u_T}{\partial D} + \frac{\partial L}{\partial u_S}\frac{\partial u_S}{\partial D} \tag{20}$$

Equation (20) can also be expressed in matrix from:

$$\frac{dL}{dD} = \frac{\partial L}{\partial D} + \begin{bmatrix} \frac{\partial L}{\partial u_x} & \frac{\partial L}{\partial u_F} & \frac{\partial L}{\partial u_T} & \frac{\partial L}{\partial u_S} \end{bmatrix} \begin{bmatrix} \frac{\partial u_x}{\partial D} \\ \frac{\partial u_F}{\partial D} \\ \frac{\partial u_T}{\partial D} \\ \frac{\partial u_S}{\partial D} \end{bmatrix} \tag{21}$$

The governing nonlinear equations of each discipline in residual form are:

$$R_x\big(D, u_x(D), x_{surf}(D)\big) = 0 \tag{22}$$

$$R_F\big(D, u_F(D), T_{surf}(D), u_x(D)\big) = 0 \tag{23}$$

$$G_S(F_B(u_F(D), u_x(D))) = 0 \tag{24}$$

$$G_T\big(H_B(u_F(D), u_x(D))\big) = 0 \tag{25}$$

$$R_S(D, u_S(D), F_B(u_F(D), u_x(D))) = 0 \tag{26}$$

$$R_T\big(D, u_T(D), H_B(u_F(D), u_x(D))\big) = 0 \tag{27}$$

$$G_S'\big(x_{surf}(D), u_S(D)\big) = 0 \tag{28}$$

$$G_T'\big(T_{surf}(D), u_T(D)\big) = 0 \tag{29}$$

where R_x, R_F, R_S, R_T, represent the residuals of the mesh deformation, fluid, elastic, and thermal analysis problem, respectively. In the above equations, variables G_S, G_S', G_T, G_T' represent the residuals of the FSI equations for aero-elastic and aero-thermal data transfer, respectively. $F_B(u_F, u_x)$ represents pointwise surface forces, and $H_B(u_F, u_x)$ represents pointwise surface heat fluxes. In order to make this a general case, we are assuming that the residual from each domain, also depends on the design variable *D*.

Taking into account the governing nonlinear equations of each discipline in residual form as given previously in Eq. (22) - Eq. (29), the individual disciplinary sensitivities at one single time step are found to be the solution of the following coupled system of equations:

$$\begin{bmatrix} \frac{\partial R_x}{\partial u_x} & 0 & 0 & 0 & 0 & 0 & 0 & 0 & \frac{\partial R_x}{\partial x_{surf}} & 0 \\ \frac{\partial R_F}{\partial u_x} & \frac{\partial R_F}{\partial u_F} & 0 & 0 & 0 & 0 & 0 & 0 & 0 & \frac{\partial R_F}{\partial T_{surf}} \\ -\frac{\partial F_B}{\partial u_x} & -\frac{\partial F_B}{\partial u_f} & I & 0 & 0 & 0 & 0 & 0 & 0 & 0 \\ -\frac{\partial H_B}{\partial u_x} & -\frac{\partial H_B}{\partial u_F} & 0 & I & 0 & 0 & 0 & 0 & 0 & 0 \\ 0 & 0 & \frac{\partial G_S}{\partial F_B} & 0 & I & 0 & 0 & 0 & 0 & 0 \\ 0 & 0 & 0 & \frac{\partial G_T}{\partial H_B} & 0 & I & 0 & 0 & 0 & 0 \\ 0 & 0 & 0 & 0 & \frac{\partial R_S}{\partial G_S} & 0 & \frac{\partial R_S}{\partial u_S} & 0 & 0 & 0 \\ 0 & 0 & 0 & 0 & 0 & \frac{\partial R_T}{\partial G_T} & 0 & \frac{\partial R_T}{\partial u_T} & 0 & 0 \\ 0 & 0 & 0 & 0 & 0 & 0 & \frac{\partial G'_S}{\partial u_S} & 0 & \frac{\partial G'_S}{\partial x_{surf}} & 0 \\ 0 & 0 & 0 & 0 & 0 & 0 & 0 & \frac{\partial G'_T}{\partial u_T} & 0 & \frac{\partial G'_T}{\partial T_{surf}} \end{bmatrix} \begin{bmatrix} \frac{du_x}{dD} \\ \frac{du_F}{dD} \\ \frac{dF_B}{dD} \\ \frac{dH_B}{dD} \\ \frac{dG_S}{dD} \\ \frac{dG_T}{dD} \\ \frac{du_S}{dD} \\ \frac{du_T}{dD} \\ \frac{dx_{surf}}{dD} \\ \frac{dT_{surf}}{dD} \end{bmatrix} = \begin{bmatrix} -\frac{\partial R_x}{\partial D} \\ -\frac{\partial R_F}{\partial D} \\ 0 \\ 0 \\ 0 \\ 0 \\ -\frac{\partial R_S}{\partial D} \\ -\frac{\partial R_T}{\partial D} \\ 0 \\ 0 \end{bmatrix} \tag{30}$$

In Eq. (30), the first and second equations correspond to equations for the mesh and flow variable sensitivities, respectively. The third and fourth equations correspond to the construction of the surface force and heat flux sensitivities, given the previous two sensitivities. The fifth and sixth equations correspond to the sensitivity of the FSI transfer from the fluid domain to the structural domain. The seventh and eight equations correspond to the sensitivity of the thermal and elastic solvers. Finally, the last two equations correspond to the sensitivity of the FSI transfer from the structural domain back to the flow solver.

Each disciplinary solution procedure requires the inversion of the same Jacobian matrix as the corresponding analysis problem, which is done using the same iterative solver. Furthermore, the fluid-structure coupling requires the transfer of the force and heat flux sensitivities from the flow domain to the structure domain. In return, we require the transfer of the surface displacement sensitivities and surface temperature sensitivities from the structure domain back to the fluid domain.

Solving the set of equations presented in Eq. (30) provides us with the state variable sensitivities with respect to the design variables. Now, we can substitute this into Eq. (21) and solve for the complete sensitivity vector $\frac{dL}{dD}$. It can be seen from the above equation that when calculating sensitivities with the tangent method, the linearization scales directly with the number of design variables.

The flow of information in the sensitivity analysis process for the tangent method is summarized in Fig. 2. For detailed information on the transfer of sensitivities in the structural domain refer to references [46] and [19]. When running transient aero-thermo-elastic sensitivity analysis, similar to the analysis problem, at every time step we solve a steady-state problem on the fluid domain, and a transient problem on the structure domain. Therefore, the above formulations hold for both steady-state and transient aero-thermo-elastic sensitivity analysis. The difference between the static and transient cases shows up on the structural solver. In addition, in the tangent formulation, the Jacobian matrices must be linearized with respect to the solution from the fluid and structural domain at every time step.

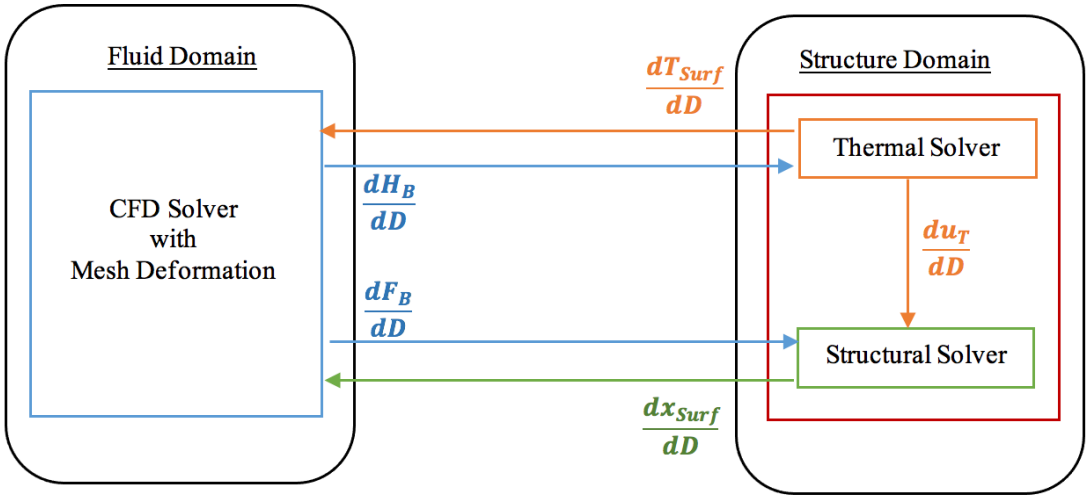

Fig. 2 Flow of information for the aero-thermo-elastic tangent sensitivity analysis.

B. Aero-Thermo-Elastic Adjoint Sensitivity Analysis

For the adjoint formulation, we require the transpose of the forward linearization as shown below:

$$\frac{dL}{dD}^T = \frac{\partial L}{\partial D}^T + \begin{bmatrix} \frac{\partial u_x}{\partial D}^T & \frac{\partial u_F}{\partial D}^T & \frac{\partial u_T}{\partial D}^T & \frac{\partial u_S}{\partial D}^T \end{bmatrix} \begin{bmatrix} \frac{\partial L}{\partial u_x}^T \\ \frac{\partial L}{\partial u_F}^T \\ \frac{\partial L}{\partial u_T}^T \\ \frac{\partial L}{\partial u_S}^T \end{bmatrix} \tag{31}$$

The corresponding adjoint problem can be obtained by pre-multiplying Eq. (31) by the inverse of the large coupling matrix, and substituting this into Eq. (21), transposing the entire system, and defining adjoint variables at one single time step as solutions to the following coupled system:

$$\begin{bmatrix} \frac{\partial R_x}{\partial u_x}^T & \frac{\partial R_F}{\partial u_x}^T & -\frac{\partial F_B}{\partial u_x}^T & -\frac{\partial H_B}{\partial u_x}^T & 0 & 0 & 0 & 0 & 0 & 0 \\ 0 & \frac{\partial R_F}{\partial u_F}^T & -\frac{\partial F_B}{\partial u_F}^T & -\frac{\partial H_B}{\partial u_F}^T & 0 & 0 & 0 & 0 & 0 & 0 \\ 0 & 0 & I & 0 & \frac{\partial G_S}{\partial F_B}^T & 0 & 0 & 0 & 0 & 0 \\ 0 & 0 & 0 & I & 0 & \frac{\partial G_T}{\partial H_B}^T & 0 & 0 & 0 & 0 \\ 0 & 0 & 0 & 0 & I & 0 & \frac{\partial R_S}{\partial G_T}^T & 0 & 0 & 0 \\ 0 & 0 & 0 & 0 & 0 & I & 0 & \frac{\partial R_T}{\partial G_T}^T & 0 & 0 \\ 0 & 0 & 0 & 0 & 0 & 0 & \frac{\partial R_S}{\partial u_S}^T & 0 & \frac{\partial G'_S}{\partial u_S}^T & 0 \\ 0 & 0 & 0 & 0 & 0 & 0 & 0 & \frac{\partial R_T}{\partial u_T}^T & 0 & \frac{\partial G'_T}{\partial u_T}^T \\ \frac{\partial R_x}{\partial x_{surf}}^T & 0 & 0 & 0 & 0 & 0 & 0 & 0 & \frac{\partial G'_S}{\partial x_{surf}}^T & 0 \\ 0 & \frac{\partial R_F}{\partial T_{surf}}^T & 0 & 0 & 0 & 0 & 0 & 0 & 0 & \frac{\partial G'_T}{\partial T_{surf}}^T \end{bmatrix} \begin{bmatrix} \Lambda_{u_x} \\ \Lambda_{u_F} \\ \Lambda_{F_B} \\ \Lambda_{H_B} \\ \Lambda_{G_S} \\ \Lambda_{G_T} \\ \Lambda_{u_S} \\ \Lambda_{u_T} \\ \Lambda_{x_{surf}} \\ \Lambda_{T_{surf}} \end{bmatrix} = \begin{bmatrix} \frac{\partial L}{\partial u_x}^T \\ \frac{\partial L}{\partial u_F}^T \\ 0 \\ 0 \\ 0 \\ \frac{\partial L}{\partial u_S}^T \\ \frac{\partial L}{\partial u_T}^T \\ 0 \\ 0 \\ 0 \end{bmatrix} \tag{32}$$

Once again, the solution of the various disciplinary adjoint equations requires the inversion of the corresponding disciplinary Jacobians (transposed in this case) which can be accomplished using the same iterative solvers as for the analysis and forward sensitivity problems. Additionally, the input to the structural adjoint problem consists of the variables $\Lambda_{x_{surf}}$ and $\Lambda_{T_{surf}}$, which have the same dimensions as the surface displacements and temperatures output from the structural analysis solver. On the other hand, the output of the structural adjoint solver consists of the variables Λ_{F_B} and Λ_{H_B}, which are of the same dimension as the force and heat flux inputs to the structural solver in the analysis problem, respectively. Once the vector of adjoint variables for each discipline is available, it may be substituted into the total sensitivity equation as:

$$\frac{dL}{dD}^T = \frac{\partial L}{\partial D}^T + \begin{bmatrix} -\frac{\partial R_x}{\partial D}^T & -\frac{\partial R_F}{\partial D}^T & -\frac{\partial R_T}{\partial D}^T & -\frac{\partial R_S}{\partial D}^T \end{bmatrix} \begin{bmatrix} \Lambda_x \\ \Lambda_F \\ \Lambda_T \\ \Lambda_S \end{bmatrix} \tag{33}$$

Again, it is clear from the above equations that the number of design variables only affects the matrix-vector products at the end of the computation process [65].

The flow of information for the sensitivity analysis process using the adjoint method is summarized in Fig. 3. For a detailed description of transfer of sensitivities in the solid domain refer to reference [46] and [19] . When running transient aero-thermo-elastic sensitivity analysis, similar to the analysis problem, we solve a steady-state problem on the fluid domain at each time step and a transient problem on the structure domain. Additionally, we require the solution history for both the fluid and structure domain at each time step, due to the fact that the corresponding Jacobian linearizations are performed about the current state. Therefore, first the analysis is run and the structural and flow solution at each time step is written to file and then during the adjoint reverse time integration, these solutions are read back from disk.

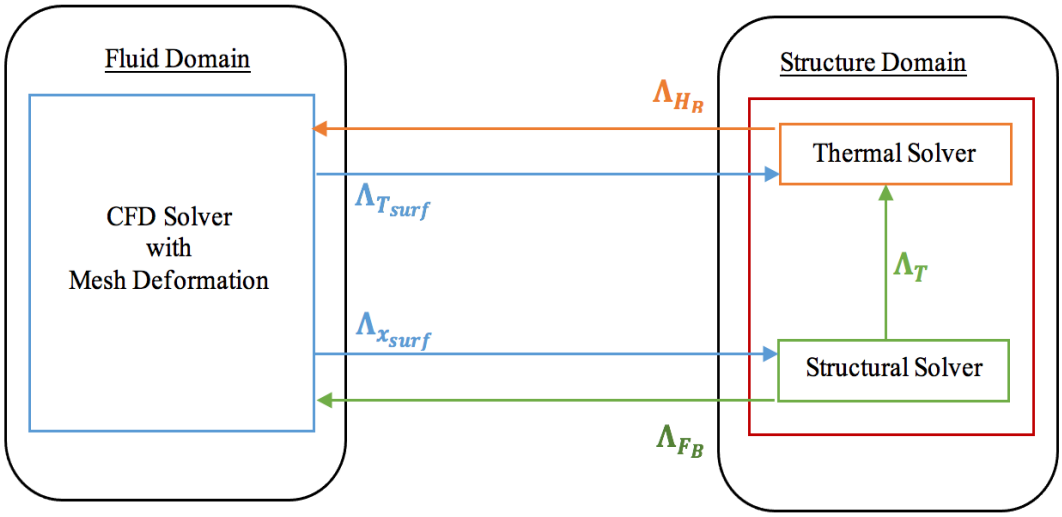

Fig. 3 Transfer of information for the coupled aero-thermo-elastic adjoint sensitivity analysis.

V. Aero-Thermo-Elastic Numerical Results

In this section, we first present solutions for the aero-thermo-elastic analysis of an aerodynamically heated panel case. Next, this heated panel case is used to verify the thermo-elastic sensitivities in AStrO. Then the aero-thermo-elastic sensitivities of the coupled platform described in the earlier section are verified using this panel case. Finally, the verified coupled adjoint-based sensitivities are used to perform aero-thermo-elastic optimizations on the panel.

A. An Overview of Wind Tunnel Experiment for the Heated Panel

A schematic of a proposed experiment that could be used to validate the flow/thermal/structural analysis as presented in reference [66] is shown in Fig. 4. Here, we consider the case where the panel is supported by immovable supports on the bottom corners, and the panel deforms into a convex shape as shown in Fig. 4.

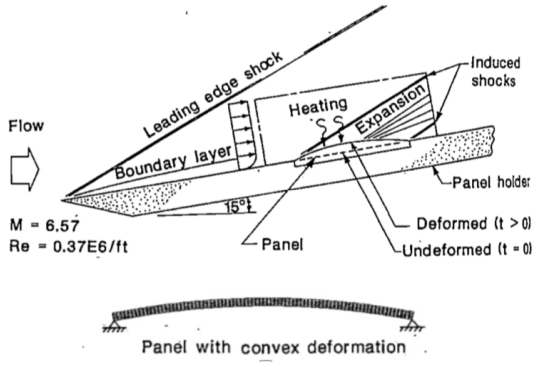

Fig. 4 Schematic diagram of the experiment that can be used to validate the flow/thermal/structural analysis of the heated panel reproduced from reference [66].

B. Summary of the Applied Numerical Boundary Conditions for the Heated Panel

The boundary conditions applied to the coupled problem are summarized in Fig. 5. The top surface of the panel, which is the fluid/structure interface, has a surface heat flux applied on the structure side, and an applied temperature enforced from the structure side on to the fluid side. The sides of the panel are considered isothermal, with an applied temperature of 530R. The bottom surface of the panel is insulated. The panel is fixed on the left and right edges of the bottom surface [66, 67].

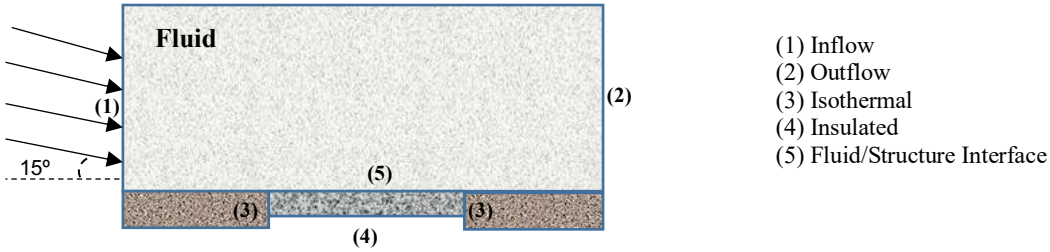

Fig. 5 Applied boundary conditions for the aero-thermo-elastic problem of a heated panel.

The initial free-stream flow parameters for this case are described in Table 1 [66]. The flow has an incidence of 15 degrees with regards to the panel as shown in Fig. 5. The fluid mesh used for this study has 2,474,940 nodes, with 4,725,000 prism elements. The fluid mesh has a wall spacing of 6×10^{-6}, which gives a y^+ of less than one along the panel surface.

Table 1 Initial free-stream conditions for the coupled flow over the heated panel.

Free-stream conditions	***Value***
Free-stream Mach number (Ma_∞)	6.57 (dimensionless)
Wall temperature (T_w)	530 R
Free-stream Reynolds number (Re_∞)	0.37×10^6 1/ft
Free-stream temperature (T_∞)	530 K
Free-stream velocity (U_∞)	6612.3 ft/s
Free-stream pressure (P_∞)	0.0971 psi

The test panel is 4in long, has a thickness of 0.1in, and a width of 0.5in. It is made from AM-350 stainless steel. The properties for the panel are tabulated in Table 2 [66]. The structure mesh used in this coupled simulation has 3,216 nodes, with 1,995 hexahedral elements.

Table 2 Panel material properties [66].

Property	***Value***
Density *(ρ)*	0.282 lbm/in^3
Thermal Conductivity *(k)*	0.12864×10^{-3} *BTU/(s.in.R)*
Specific heat capacity *(C)*	0.11162 *BTU/(lbm.R)*
Thermal expansion (α)	0.62643×10^{-5} *1/R*
Modulus of elasticity (E)	0.35346×10^{8} lbf/in^2
Poisson's ration (ν)	0.25 (dimensionless)

Since the flow field reaches equilibrium much faster than the thermal response of the panel structure, the coupled problem is solved as a steady-state problem on the fluid side and as a transient problem on the structural side. The time step for the thermal solver is taken as 5*s*. Thus, it takes six coupled cycles between the fluid and structure solvers to reach the transient solution at thirty seconds.

C. Aero-thermo-elastic Analysis Results for the Heated Panel

In this section, numerical results from the aero-thermo-elastic analysis of the panel with the convex deformation are presented. The interaction between the panel deformation and the flow density distributions at t = 30*s* for the convex panel is shown in Fig. 6, which plots computed values of density non-dimensionalized by the freestream density. Although, the test cases are 2D in nature, the calculations are done fully in 3D. Hence, we have plotted the solution with a slight perspective to show the full computational domain. The figure clearly shows the development of a shock originating from the left support on the windward side. The density of the fluid increases through this shock at first but then decreases as the flow expands over the convex panel. A recompression shock is developed as the flow is turned by the deformed panel near the right side. These results agree well qualitatively with the computational solutions presented in reference [66]. In reference [11], we did a detailed comparison of the numerical results for this case against available analytical solutions. For more details on the aero-thermo-elastic results for this case and other cases, please refer to the reference [11].

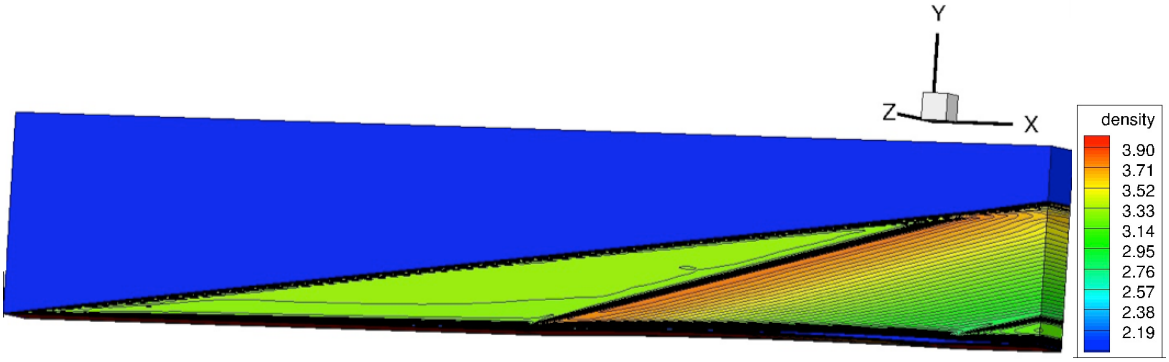

Fig. 6 Flow density distributions at t = 30s, for the heated panel with convex deformation.

D. Thermo-Elastic Sensitivity Analysis Verification for the Heated Panel

Previously, we mentioned that AStrO has the capability to calculate exact sensitivities using the adjoint method. In this section we show verification for these sensitivities for the thermo-elastic simulation of the heated panel case.

A schematic of the computational model and boundary conditions for the thermo-elastic heated panel problem is shown in Fig. 7. The boundary conditions are the same as the aero-thermo-elastic heated panel case. The panel is supported by immovable supports on the left and right edges of the bottom surface. The bottom surface of the panel is insulated, while the faces on the right and left side of the panel have a constant temperature equal to the initial temperature of 530*R*. In the thermo-elastic simulation, a uniform heat flux is applied to the top surface of the panel to mimic the aerodynamic heating of the panel. Under these thermal and structural boundary conditions, similar to the aero-thermo-elastic analysis, the panel deforms into a convex shape [66, 67].

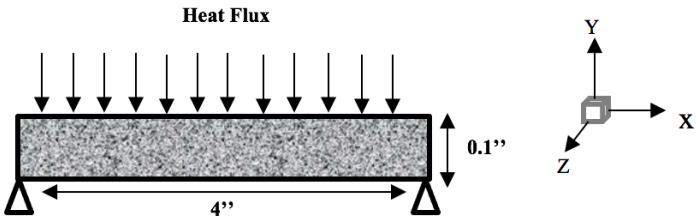

Fig. 7 Coupled thermal/structural model and boundary conditions for a heated panel reproduced from reference [35].

The material properties of the panel are the same as the panel used in the aero-thermo-elastic analysis problem. These properties were summarized in Table 2 [66]. The mesh used in this study is the same as the structure mesh used in the aero-thermo-elastic analysis problem presented in the previous section.

Since we are studying the solution at early times, the heat flux across the panel is nearly uniform, and can be approximated by the following equation [66]:

$$q(t) = 0.026 - 0.0001t\ (\frac{BTU}{in^2.s}) \tag{34}$$

Equation (34) is used as a thermal boundary condition in order to mimic the aerodynamic heating for the thermo-elastic validation. The time step used for the coupled thermo-elastic analysis is 1s. Hence 30 time steps were required to heat the panel for 30s.

When dealing with thermo-elastic sensitivity analysis, we need to transfer sensitivities between the thermal and structural solvers. The transfer of information performed by AStrO during a sensitivity analysis for both the tangent and the adjoint method are summarized in in Fig. 8. The one-way dependence between the elastic displacement on temperature distribution is clear in this figure. More details regarding the sensitivity analysis formulations and implementations in AStrO are given in reference [46].

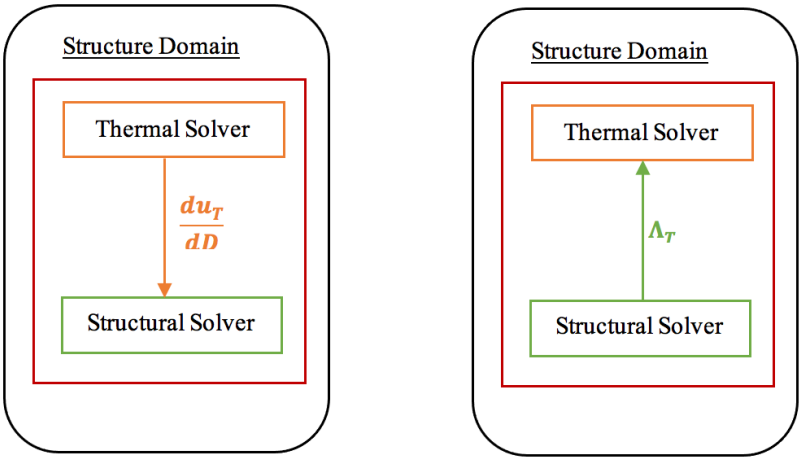

Fig. 8 Flow of information for the thermo-elastic tangent (on the left) and adjoint (on the right) sensitivity analysis process in AStrO

For this case, the objective function is defined using the deformation of the panel in the x- and y-directions, as shown below:

$$L = \sum_{i=1}^{n}(Disp\_x(i))^2 + (Disp\_y(i))^2 \tag{35}$$

where 'i' is the node number and 'n' is the total number of nodes in the panel.

In order to test the adjoint-based sensitivities, the elastic modulus, the thermal conductivity, the coefficient of thermal expansion, and the specific heat capacity of the panel material were defined as the design variables. The sensitivity of each property was scaled to the original value, resulting in the following design-dependent definitions:

$$\begin{cases} E = E_0 + 10^7\, D_1 \\ k = k_0 + 10^{-4} D_{\,2} \\ \alpha = \alpha_0 + 10^{-6} D_3 \\ C = C_0 + 10^{-1} D_4 \end{cases} \tag{36}$$

The adjoint-based sensitivities were verified against the sensitivities calculated by the tangent method and complex-step method [68]. Tables 3 through Table 6 show a comparison of coupled thermo-elastic sensitivities obtained from the complex analysis run with those of the tangent and adjoint linearization for 6 different time steps. Each table presents results for one of the design variables defined in Eq. (36). As shown in these tables, the sensitivity values from the tangent and adjoint linearization match with the complex-step method to machine precision. For more details on this case and other thermo-elastic sensitivity analysis and optimization cases please refer to previous work [12, 19].

Table 3 Comparison of objective sensitivities for the heated panel for the adjoint, tangent and complex-step methods for design variable D_1 as defined in Eq. (36).

Time step	*Adjoint*	*Tangent*	*Complex*
5	-0.0005658745509	-0.0005658745509	-0.0005658745510
10	-0.0041847191992	-0.0041847191992	-0.0041847191996
15	-0.0132425156473	-0.0132425156472	-0.0132425156484
20	-0.0297337370432	-0.0297337370432	-0.0297337370458
25	-0.0553518559203	-0.0553518559203	-0.0553518559249
30	-0.0915353372070	-0.0915353372071	-0.0915353372147

Table 4 Comparison of objective sensitivities for the heated panel for the adjoint, tangent and complex-step methods for design variable D_2 as defined in Eq. (36).

Time step	*Adjoint*	*Tangent*	*Complex*
5	-0.0270281059525	-0.0270281059525	-0.0270281059525
10	-0.1424427208577	-0.1424427208577	-0.1424427208578
15	-0.4235076821464	-0.4235076821462	-0.4235076821465
20	-0.9637033879671	-0.9637033879673	-0.9637033879675
25	-1.8656308994337	-1.8656308994336	-1.8656308994339
30	-3.2372661777168	-3.2372661777178	-3.2372661777184

Table 5 Comparison of the objective sensitivities for the heated panel for the adjoint, tangent and complex-step methods for design variable D_3 as defined in Eq. (36).

Time step	*Adjoint*	*Tangent*	*Complex*
5	0.0644539160860	0.0644539160860	0.0644539160860
10	0.4214617163555	0.4214617163556	0.4214617163557
15	1.2889374961929	1.2889374961924	1.2889374961929
20	2.8522092885360	2.8522092885354	2.8522092885367
25	5.2696838576481	5.2696838576459	5.2696838576481
30	8.6764603110799	8.6764603110797	8.6764603110834

Table 6 Comparison of objective sensitivities for the heated panel for the adjoint, tangent and complex-step methods for design variable D_4 as defined in Eq. (36).

Time step	*Adjoint*	*Tangent*	*Complex*
5	-0.3298385175240	-0.3298385175243	-0.3298385175244
10	-2.1963367650602	-2.1963367650602	-2.1963367650615
15	-6.7320990871707	-6.7320990871682	-6.7320990871707
20	-14.8687791829420	-14.8687791829394	-14.8687791829461
25	-27.3767070817806	-27.3767070817733	-27.3767070817816
30	-44.8893798636163	-44.8893798636146	-44.8893798636355

E. Aero-Thermo-Elastic Sensitivity Analysis Verification for the Heated Panel with Mach = 0.8

To verify the aero-thermo-elastic adjoint-based sensitivities, the case of flow with Mach = 0.8 over the panel is considered. This is done, since the case of flow with Mach = 6.57 over this panel does not fully converge due to limiter unsteadiness. In addition, the limiters are considered frozen in the sensitivity analysis and are not linearized in the current tangent/adjoint implementation. Therefore, using the case of flow with Mach = 0.8 over the panel, allows us to sidestep the effect of limiters in the sensitivity verification. Additionally, the time-dependent heat flux boundary condition which approximates the heat flux from the flow field given by Eq. (34) is employed. This approach was used due to the appearance of inconsistent sensitivities in the heat flux routine which remained unresolved at the time of publication. However, this test case employs an aerodynamic objective coupled with structural design variables, thus providing a test of the coupled aero-thermo-elastic sensitivities. The adjoint linearization is verified using the duality relation [50] to the tangent approach, while the tangent sensitivities are verified with the finite-difference method [41, 68].

The aerodynamic objective function for this case is based on the computed drag of the panel. Since the flow has an angle of attack of 15°, a function of the force coefficient in the *x*-direction (aligned with the panel) is used as the objective rather than C_D itself. Specifically, the objective L is defined as Eq. (37).

$$L = (C_x)^2 \tag{37}$$

In order to test the adjoint-based sensitivities, the thermal conductivity and thickness of the panel are defined as the design variables as presented in Eq. (38).

$$\begin{cases} k = k_0 + 10^{-4} D_1 \\ Thickness = Thickness_{intial} \times D_2 \end{cases} \tag{38}$$

The adjoint based sensitivities were verified against the sensitivities calculated by the tangent and finite-difference methods. Table 7 and Table 8 show a comparison of the coupled aero-thermo-elastic sensitivities for flow over the panel obtained from the finite-difference analysis run with those of the tangent and adjoint linearization. Table 7 and Table 8 show results for the case of using thermal conductivity and thickness of the panel as design variables, respectively. Each table has results for different number of time steps. The sensitivities of the objective function match down to machine precision between the tangent and the adjoint. These sensitivities match reasonably well with the sensitivities calculated through the finite-difference method. As can be seen in both Table 7 and Table 8, the sensitivity values are increasing with the number of time steps. This is to be expected, since as time passes the panel deforms more and the drag increases.

Table 7 Comparison of the sensitivity of the objective function defined in Eq. (37) with respect to the design variable D_1 defined in Eq. (38), for the heated panel in Mach = 0.8 flow, at different coupling time steps.

Time Step	*Adjoint*	*Tangent*	*Finite-Difference*
1	-3.47763135461**56**$\times 10^{-6}$	-3.47763135461**82**$\times 10^{-6}$	-3.6066387221$\times 10^{-6}$
2	-5.31123417602**13**$\times 10^{-6}$	-5.31123417602**95**$\times 10^{-6}$	-5.6107710055$\times 10^{-6}$
3	-6.04453180932**982**$\times 10^{-6}$	-6.04453180933**126**$\times 10^{-6}$	-7.3720293562$\times 10^{-6}$
5	-6.92850553411**629**$\times 10^{-6}$	-6.92850553411**926**$\times 10^{-6}$	-7.6129645635$\times 10^{-6}$

Table 8 Comparison of the sensitivity of the objective function defined in Eq. (37) with respect to the design variable D_2 defined in Eq. (38), for the heated panel in Mach = 0.8 flow, at different coupling time steps.

Time Step	*Adjoint*	*Tangent*	*Finite-Difference*
1	-6.96927382827**343**$\times 10^{-6}$	-6.96927382827**098**$\times 10^{-6}$	-7.3292648685$\times 10^{-6}$
2	-2.09733547485**967**$\times 10^{-5}$	-2.09733547486**444**$\times 10^{-5}$	-2.2907747595$\times 10^{-5}$
3	-4.19421030208**063**$\times 10^{-5}$	-4.19421030209**051**$\times 10^{-5}$	-4.6948589964$\times 10^{-5}$
5	-8.98882633197**205**$\times 10^{-5}$	-8.98882633195**547**$\times 10^{-5}$	-10.648608982$\times 10^{-5}$

F. Aero-Thermo-Elastic Design Optimization for the Heated Panel in Hypersonic Flow

Next, the verified adjoint-based sensitivities are used in the aero-thermo-elastic optimization of the heated panel case in hypersonic flow. The initial free-stream flow parameters for this case were given previously in Table 1. The optimization is first performed for one coupled time step. Later, the optimization is repeated taking into account five coupled time steps. A time step of one second is used. For the optimization cases presented in the coming pages, the SNOPT [69] sequential quadratic programming algorithm is used to drive the constrained optimization.

The objective function defined for this problem is shown below:

$$L(t) = (C_x(t_{final}))^2 + n_{element} \times (k_{t_{final}} - \left(k_{t_{initial}} + 0.000072\right))^2 \\ 10^{-4} \times (Mass_{t_{final}} - 2.5 \times Mass_{t_{intial}})^2 \quad (39)$$

In Eq. (39), a penalty is put on the mass and the thermal conductivity of the panel. Weights are applied to approximately balance the influence of the various terms of the objective function in the optimization process. The goal in this optimization problem is to minimize the objective function presented in Eq. (39) with respect to the thermal conductivity and the thickness of the panel as shown below:

$$\begin{cases} k = k_0 + 10^{-4} D_1 \\ Thickness = Thickness_{intial} \times D_2 \end{cases} \quad (40)$$

1. *Aero-Thermo-Elastic Design Optimization for the Heated Panel in Mach 6.57 flow, for One Coupled Time Step*

For this optimization problem NSU3D and AStrO are run for only one time step during the optimization process. The optimization was performed using SNOPT. The optimum value of the design variables, which reflect the changes in the material properties of the panel, are summarized in Table 9. The change in the objective function from the baseline panel to the aero-thermo-elastically optimized panel case is shown in Table 10.

Table 9 Optimum design variables, initial and optimized material properties of the heated panel in Mach 6.57 flow, with one coupled time step.

Design Variable		***Material Properties***	***Initial Material Properties***	***Optimized Material Properties***
$\boldsymbol{D_1}$	*0.7645006*	***Thermal Conductivity***	0.00012864 *BTU/(s.in.R)*	0.0002059 *BTU/(s.in.R)*
$\boldsymbol{D_2}$	*2.504113*	***Thickness***	1 *in*	*2.504113 in*

Table 10 Comparison of the baseline and aero-thermo-elastically optimized objective function for the heated panel in Mach 6.57 flow, with one coupled time step.

	Baseline	***Aero-Thermo-elastic optimization***
Objective function (*Eq. (39)*)	1.6722326×10^{-4}	7.8904212×10^{-5}

The convergence of the optimization process for the panel case is shown in Fig. 9. The optimization is run for 10 design steps during which the value of the objective function is reduced approximately by a factor of two.

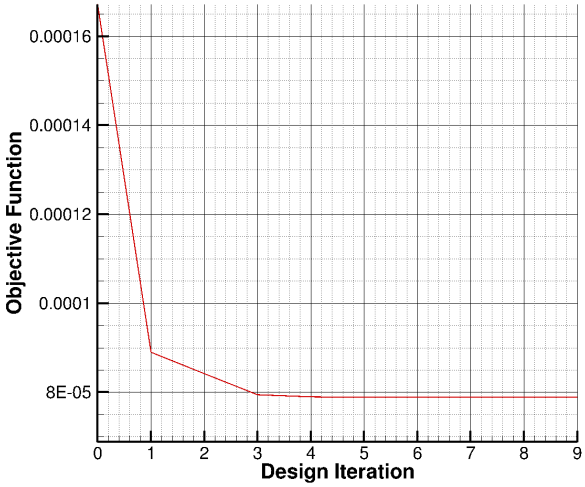

Fig. 9 Convergence of the aero-thermo-elastic optimization process for the heated panel case in Mach 6.57 flow, with one coupled time step.

2. *Aero-Thermo-Elastic Design Optimization for the Heated Panel with Mach 6.57, for Five Coupled Time Steps*

For this optimization problem NSU3D and AStrO are run for five time steps during the optimization process. The objective function and design variables are similar to the case with a single time step but correspond to the values at the final time step. Therefore, Eq. (39) is used as the objective function and Eq. (40) defines the design variables used for this case.

The optimum value of the design variables, which reflect the changes in the material properties of the panel, are summarized in Table 11. In addition, Table 12 shows the change in the objective function from the baseline panel to the aero-thermo-elastically optimized panel case. Comparing the optimized material properties from Table 9 with Table 11, it can be observed that the values for the optimized material properties are slightly higher for the optimization using five coupled time steps compared to the optimization using a single time step. This behavior is expected since the aerodynamic term in the objective function is initially larger for the case with five time steps. This is similar to the increase in the sensitivities with the number of time steps seen in Table 7 and Table 8

Table 11 Optimum design variables, initial and optimized material properties of the heated panel in Mach 6.57 flow, with five coupled time steps.

Design Variable		***Material Properties***	***Initial Material Properties***	***Optimized Material Properties***
D_1	*0.8556365*	***Thermal Conductivity***	0.00012864 *BTU/(s.in.R)*	*0.000214203 BTU/(s.in.R)*
D_2	*2.5134456*	***Thickness***	1 *in*	*2.5134456 in*

Table 12 Comparison of the baseline and aero-thermo-elastically optimized objective function for the heated panel in Mach 6.57 flow, with five coupled time steps.

	Baseline	***Aero-Thermo-elastic optimization***
Objective function (*Eq. (39)*)	2.2976563×10^{-4}	1.1060668×10^{-4}

The convergence of the optimization process for the panel case using five time steps is shown in Fig. 10. Overall, the convergence of the optimization process is similar for this case compared to the previous case using a single time step. The simulations were performed on the Teton supercomputer at University of Wyoming Advanced Research Computing Center (ARCC) and required approximately 20 hours on 320 cores.

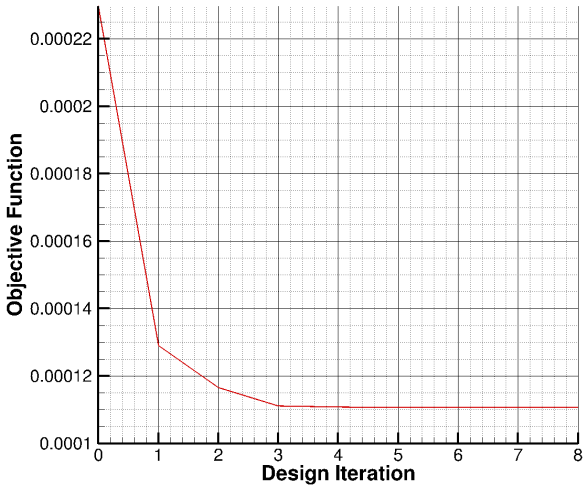

Fig. 10 Convergence of the aero-thermo-elastic optimization process for the heated panel case in Mach 6.57 flow, with five coupled time steps.

The interaction between the panel deformation and the flow density distributions at t = 30*s* for the aero-thermo-elastically optimized panel design using five time steps is shown in Fig. 11. In this figure, the computed values of density are non-dimensionalized by the free-stream density. The outcome of the optimization becomes more apparent if we compare Fig. 11 to Fig. 6, presented previously for the baseline panel case .We can clearly see the strength of the shocks and flow disturbances are reduced in the flow over the optimized panel in comparison to the flow over the baseline panel.

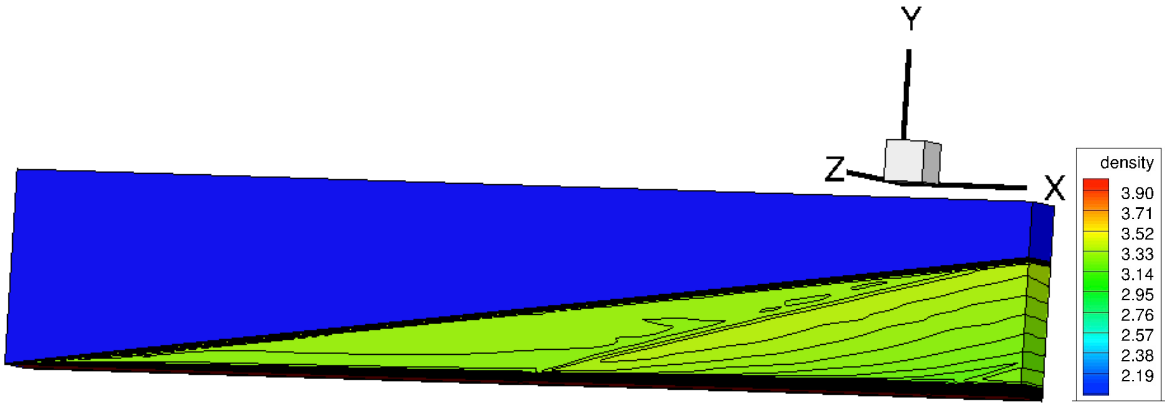

Fig. 11 Flow density distributions at t = 30*s*, for the aero-thermo-elastically optimized panel design.

VI. Conclusion

In previous work, a loosely coupled, three-dimensional, aero-thermo-elastic analysis platform was developed and validated. The platform uses the following modules developed in-house and tested previously: the flow solver NSU3D, the thermo-elastic capability from the structural solver AStrO, the FSI module, and the mesh deformation capability. In this work, the aero-thermo-elastic platform, which consists of high-fidelity solvers for each discipline, was further developed for design optimization. AstrO's thermo-elastic sensitivity analysis capabilities and NSU3D's flow sensitivity analysis capabilities, have been validated in previous work. The main challenge here centered around coupling the disciplinary sensitivities from these two platforms for coupled aero-thermo-elastic optimization. Both tangent-based and adjoint-based aero-thermo-elastic sensitivities were implemented. The adjoint-based sensitivities are shown to be consistent with direct differentiation or the tangent method. Also, preliminary adjoint-based optimization results are promising. For the aero-thermo-elastic panel problem used in this paper for sensitivity verification and optimization, a fixed heat flux was prescribed on the structure domain due to inconsistencies encountered with the linearization of the heat flux routine. Current work is ongoing to enable the inclusion of these sensitivities in the coupled aero-thermo-elastic optimization framework. The developed aero-thermo-elastic analysis

and design platform should enable new opportunities for design and understanding of physics in high-speed flows and hypersonic vehicle design.

Acknowledgments

This work is supported by ONR Grant N00014-17-1-2337. We are grateful for computer time provided by the NCAR-Wyoming Supercomputer Center (NWSC) and by the University of Wyoming Advanced Research Computing Center (ARCC).

References

[1] Jameson, A., Martinelli, L., and Pierce, N. A. "Optimum Aerodynamic Design Using the Navier-Stokes Equations," *Theoretical and Computational Fluid Dynamics* Vol. 10, No. 1-4, 1998, pp. 213-237. doi: 10.1007/s001620050060

[2] Witherden, F. D., and Jameson, A. "Future Directions of Computational Fluid Dynamics," 23rd AIAA Computational Fluid Dynamics Conference, Denver, Colorado, 2017, AIAA 2017-3791. doi: 10.2514/6.2017-3791

[3] Fife, M. E., and Davis, R. L. "A Conjugate Heat Transfer Rans/Des Simulation Procedure," 47th AIAA Aerospace Sciences meeting Orlando, Florida, 2009, AIAA 2009-913. doi: 10.2514/6.2009-913

[4] Reinert, J. D., Dwivedi, A., and Candler, G. V. "Verification of a Conjugate Heat Transfer Tool with US3D," AIAA SciTech 2019, San Diego, California, 2019, AIAA 2019-1892. doi: 10.2514/6.2019-1892

[5] Seager, C., and Agarwal, R. K. "Hypersonic Blunt-Body Shape Optimization for Reducing Drag and Heat Transfer," *Journal of Thermophysics and Heat Transfer* Vol. 31, No. 1, 2017, pp. 48-55. doi: 10.2514/1.t4650

[6] Nordstrom, J., and Berg, J. "Conjugate Heat Transfer for the Unsteady Compressible Navier-Stokes Equations Using a Multi-Block Coupling," *Computers & Fluids* Vol. 72, 2013, pp. 20-29. doi: 10.1016/j.compfluid.2012.11.018

[7] Errera, M. P., and Baque, B. "A Quasi-Dynamic Procedure for Coupled Thermal Simulations," *International Journal for Numerical Methods in Fluids* Vol. 72, No. 11, 2013, pp. 1183-1206. doi: 10.1002/fld.3782

[8] Dechaumphai, P., Thornton, E. A., and Wieting , A. R."Fluid-Thermal-Structural Study of Aerodynamically Heated Leading Edges," NASA Technical Memorandum, NASA, Langley Research Center , Hampton, Virginia, 1988.

[9] Zhao, X., Sun, Z., Tang, L., and Zheng, G. "Coupled Flow-Thermal-Structural Analysis of Hypersonic Aerodynamically Heated Cylindrical Leading Edge," *Engineering Applications of Computational Fluid Mechanics* Vol. 5, No. 2, 2011, pp. 170-179. doi: 10.1080/19942060.2011.11015361

[10] Maute, K., Nikbay, M., and Farhat, C. "Coupled Analytical Sensitivity Analysis and Optimization of Three-Dimensional Nonlinear Aeroelastic Systems," *AIAA Journal* Vol. 39, No. 11, 2001, pp. 2051-2061. doi: 10.2514/2.1227

[11] Kamali, S., Mavriplis, D. J., and Anderson, E. "Development and Validation of a High-Fidelity Aero-Thermo-Elastic Analysis Capability," AIAA SciTech 2020 Forum, Orlando, Florida, 2020, AIAA 2020-1449. doi: 10.2514/6.2020-1449

[12] Kamali, S., Mavriplis, D. J., and Anderson, E. "Sensitivity Analysis for Aero-Thermo-Elastic Problems Using the Discrete Adjoint Approach," AIAA Aviation 2020 Forum, Virtual event, 2020, AIAA 2020-3138. doi: 10.2514/6.2020-3138

[13] Reinert, J. D., Nompelis, I., and Candler, G. V. "Coupled Conjugate Heat Transfer Simulation for a Scramjet Inlet at Mach 8," 23rd AIAA Computatonal Fluid Dynamics Conference, Denver, Colorado, 2017, AIAA 2017-4502. doi: 10.2514/6.2017-4502

[14] Smith, L. J., Halim, L. J., Kennedy, G., and Smith, M. J. "A High-Fidelity Coupling Framework for Aerothermoelastic Analysis and Adjoint-Based Gradient Evaluation," AIAA SciTech 2021 Forum, Virtual event, 2021, AIAA-2021-0407. doi: 10.2514/6.2021-0407

[15] Zope, A., D, Schemmel, A., Bhtia, M., Bhushan, S., and Collins, E. "Development and Validation of Fluid-Thermal Interaction Solver for High Fidelity Transient Simulations," AIAA Aviation 2020, Virtual event, 2020, AIAA 2020-3006. doi: 10.2514/6.2020-3006

[16] Xia, C., and Chen, W. "Gradient-Based Aerothermodynamic Optimization of a Hypersonic Wing Profile," *Procedia Engineering* Vol. 126, 2015, pp. 189-193. doi: 10.1016/j.proeng.2015.11.214

[17] Zhang, S., Chen, F., and Liu, H. "Time-Adaptive, Loosely Coupled Strategy for Conjugate Heat Transfer Problems in Hypersonic Flows," *Journal of Thermophysics and Heat Transfer* Vol. 28, No. 4, 2014, pp. 635-646. doi: 10.2514/1.t4278

[18] Kamali, S., Mavriplis, D. J., and Anderson, E. M. "Development of a High-Fidelity Aero-Thermo-Elastic Analysis Capability," *AIAA Journal*, 2021, pp. 1-15. doi: 10.2514/1.J060279

[19] Kamali, S."Development of a High-Fidelity Aero-Thermo-Elastic Analysis and Design Capability," Ph.D. Dissertation, Department of Mechanical Engineering, University of Wyoming, Laramie, Wyoming, 2021.

[20] Polle, D., Allen, C., and Rendall, T. "A Constrained Global Optimization Framework," 14th AIAA Aviation Technology , Integraiton, and operations conference, Atlanta, GA, 2014, AIAA 2014-2034. doi: 10.2514/6.2014-2034

[21] Mavriplis, D. J., Fabiano, E., and Anderson, E. "Recent Advances in High-Fidelity Multidisciplinary Adjoint-Based Optimization with the NSU3D Flow Solver Framework," 55th AIAA Aerospace Sciences Meeting, Grapevine, TX, 2017, AIAA 2017-1169. doi: 10.2514/6.2017-1669

[22] Newman, J. C., Taylor, A. C., Barnwell, R. W., Newman, P. A., and Hou, G. J. W. "Overview of Sensitivity Analysis and Shape Optimization for Complex Aerodynamic Configurations," *Journal of Aircraft* Vol. 36, No. 1, 1999, pp. 87-96. doi: 10.2514/2.2416

[23] Nielsen, E. J., and Anderson, W. K. "Aerodynamic Design Optimization on Unstructured Meshes Using the Navier-Stokes Equations," *AIAA Journal* Vol. 37, No. 11, 1999, pp. 1411-1419. doi: 10.2514/2.640

[24] Mavriplis, D. J. "Discrete Adjoint-Based Approach for Optimization Problems on Three-Dimensional Unstructured Meshes," *AIAA Journal* Vol. 45, No. 4, 2007, pp. 741-750. doi: 0.2514/1.22743

[25] Mishra, A., Mani, K., Mavriplis, D. J., and Sitraman, J. "Time Dependent Adjoint-Based Optimization for Coupled Aeroelastic Problems," 31st AIAA Applied Aerodynamic Conference, San Diego, CA, 2013, AIAA 2013-2906

[26] Jameson, A."Aerodynamic Shape Optimization Using the Adjoint Method," Von Karman Institute, Brussels, 2003.

[27] Kenway , G. K. W., and Martins, J. "Multipoint High-Fedility Aerostructural Optimization of a Transport Aircraft Configuration," *Journal of Aircraft* Vol. 51, No. 1, 2014, pp. 144-160. doi: 10.2514/1.C032150

[28] Mavriplis, D. J."Formulation and Multigrid Solution of the Discrete Adjoint Problem on Unstructured Meshes," University of Wyoming, Laramie, Wyoming, USA.

[29] Mavriplis, D. J."Time Dependent Adjoint Methods for Single and Multi-Disciplinary Problems," University of Wyoming, Laramie, Wyoming, USA, 2015.

[30] Jaiman, R. K., Jiao, X., Geubelle, P. H., and Loth, E. "Assessment of Conservative Load Transfer for Fluid-Solid Interface with Non-Matching Meshes," *International Journal for Numerical Methods in Engineering* Vol. 64, No. 15, 2005, pp. 2014-2038. doi: 10.1002/nme.1434

[31] Jiao, X. M., and Heath, M. T. "Common-Refinement-Based Data Transfer between Non-Matching Meshes in Multiphysics Simulations," *International Journal for Numerical Methods in Engineering* Vol. 61, No. 14, 2004, pp. 2402-2427. doi: 10.1002/nme.1147

[32] Cebral, J., and Loehner, R. "Conservative Load Projection and Tracking for Fluid-Structure Problems," 34th Aerospace Science meething and exhibit, Reno, NV, USA, 1996, AIAA 96-0797. doi: 10.2514/6.1996-797

[33] Cebral, J., and Lohner, R. "Conservative Load Projection and Tracking for Fluid-Structure Problems," *AIAA Journal* Vol. 35, No. 4, 1997, pp. 687-692. doi: 10.2514/2.158

[34] Roe, B., Jaiman, R., Haselbacher, A., and Geubelle, P. H. "Combined Interface Boundary Condition Method for Coupled Thermal Simulations," *International Journal for Numerical Methods in Fluids* Vol. 57, No. 3, 2008, pp. 329-354. doi: 10.1002/fld.1637

[35] Mavriplis, D. J., and Mani, K. "Unstructured Mesh Solution Techniques Using the NS3D Solver," 52nd Aerospace Sciences Meeting, National Harbor, MD, 2014, AIAA 2014-081. doi: 10.2514/6.2014-0081

[36] Mavriplis, D. J., Anderson, E., Fertig, R., and Garnish, M. "Development of a High-Fidelity Time-Dependent Aero-Structural Capability for Analysis and Design," 57th AIAA/ASCE/AHS/ASC Structures, Structural Dynamics, and Materials Conference, AIAA SciTech Forum, San Diego, California, 2016, AIAA 2016-1175. doi: 10.2514/6.2016-1175

[37] Vassberg, J. C., Tinoco, E. N., Mani, M., Zickuhr, T., Levy, D., Broderson, O. P., Eisfeld, B., Wahls, R. A., Morrison, J. H., Mavriplis, D. J., and Murayama, M. "Summary of the Fourth AIAA CFD Drag Prediction Workshop," AIAA, Chicago , IL, 2010, AIAA 2010-4547. doi: 10.2514/6.2010-4547

[38] Vassberg, J. C., Tinoco, E. N., Mani, M., Broderson, O. P., Eisfeld, B., Wahls, R. A., Morrison, J. H., Zickuhr, T., Laflin, K. R., and Mavriplis, D. J. "Abridged Summary of the Third AIAA Computational Fluid Dynamics Drag Prediction Workshop," *Journal of Aircraft* Vol. 45, No. 3, 2008, pp. 781-798. doi: 10.2514/1.30572

[39] Mavriplis, D. J., Yang, Z., and Long, M. "Results Using NSU3D for the First Aeroelastic Prediction Workshop," 51st AIAA Aerospace Sciences Meeting, Grapevine, TX, 2013, AIAA 2013-0786. doi: 10.2514/6.2013-786

[40] Mavriplis, D. J., Long, M., Lake, T., and Langlois, M. "NSU3D Results for the Second AIAA High-Lift Prediction Workshop," 52nd AIAA Aerospace Sciences Meeting, National Harbor, MD, 2014, AIAA 2014-748. doi: 10.2514/6.2014-0748

[41] Anderson, E., Bhuiyan, F. H., Mavriplis, D. J., and Fertig, R. "Adjoint-Based High-Fidelity Aeroelastic Optimization of Wind Turbine Blade for Load Stress Minimization," Wind Energy Symposium, AIAA SciTech Forum Kissimmee ,Florida, 2018, AIAA 2018-1241. doi: 10.2514/6.2018-1241

[42] Mavriplis, D. J. "Solution of the Unsteady Discrete Adjoint for Three-Dimensional Problems on Dynamically Deforming Unstructured Meshes," Proceedings of the 46th Aerospace Sciences Meeting and Exhibit, Reno , NV, 2008, AIAA 2008-0727. doi: 10.2514/6.2008-727

[43] Mani, K., and Mavriplis, D., J. "Geometry Optimization in Three-Dimensional Unsteady Flow Problems Using the Discrete Adjoint," 51st AIAA Aerospace Sciences Meeting, Grapevine, TX, 2013, AIAA 2013-0662. doi: 10.2514/6.2013-662

[44] Roe, P. L. "Approximate Riemann Solvers Parameter Vectors and Difference Schemes," *Journal of Computational Physics* Vol. 43, No. 2, 1981, pp. 357-372. doi: 10.1016/0021-9991(81)90128-5

[45] Mani, K., and Mavriplis, D. J. "Adjoint-Based Sensitivity Formulation for Fully Coupled Unsteady Aeroelasticity Problems," *AIAA Journal* Vol. 47, No. 8, 2009, pp. 1902-1915. doi: 10.2514/1.40582

[46] Anderson, E."Development of an Open-Source Capability for High-Fidelity Thermoelastic Modeling and Adjoint-Based Sensitivity Analysis of Structures," Ph.D Dissertation, Mehcnaical Engineering, Univeristy of Wyoming, Laramie, Wyoming, 2019.

[47] "Abaqus," Version 6.14-4 ed., product of Dassault Systems Simulia Corp, Providence,RI,USA, 2017.

[48] Hilber, H. M., Hughes, T. J. R., and Taylor, R. L. "Improved Numerical Dissipation for Time Integratoin Algorithms in Structural Dynamics," *Earthquake Engineering and Structuctural Dynamics* Vol. 5, 1977, pp. 283-292. doi: 10.1002/eqe.4290050306

[49] Reddy, J. N. *Energy Principles and Variational Methods in Applied Mechanics*, John Wiley & Sons, New Jersey , USA, 2002.

[50] Nocedal, J., and Wright, S. *Numerical Optimization*, Springer, Verlag, NY, 1999.

[51] Samareh, J. A. "Discrete Data Transfer Technique for Fluid-Structure Interaction," 18th AIAA Computational Fluid Dynamics Conference, Miami Florida, 2007, AIAA 2007-4309. doi: 10.2514/6.2007-4309

[52] Verstraete, T., Alsalihi, Z., and Van den Braembussche, R. A. "Numerical Study of the Heat Transfer in Micro Gas Turbines," *Journal of Turbomachinery* Vol. 129, No. 4, 2007, p. 835. doi: 10.1115/1.2720874

[53] Verstraete, T., Alsalihi, Z., and Van den Braembussche, R. A. "A Comparison of Conjugate Heat Transfer Methods Applied to an Axial Helium Turbine," *Proceedings of the Institution of Mechanical Engineers, Part A: Journal of Power and Energy* Vol. 221, No. 7, 2007, pp. 981-989. doi: 10.1243/09576509jpe385

[54] Giles, M. B. "Stability Analysis of Numerical Interface Conditions in Fluid-Structure Thermal Analysis," *International Journal for Numerical Methods in Fluids* Vol. 25, No. 4, 1997, pp. 421-436. doi: 10.1002/(Sici)1097-0363(19970830)25:4<421::Aid-Fld557>3.0.Co;2-J

[55] Joshi, O., and Leyland, P. "Stability Analysis of a Partitioned Fluid–Structure Thermal Coupling Algorithm," *Journal of Thermophysics and Heat Transfer* Vol. 28, No. 1, 2014, pp. 59-67. doi: 10.2514/1.t4032

[56] Miller, B., A."Loosely Coupled Time Integration of Fluid-Thermal-Structural Interactions in Hypersonic Flows," Ph.D Dissertation, Aeronautical and Astronautical Engineering, Ohio State University, 2015.

[57] Roget, B., and Sitaraman, J. "Wall Distance Search Algorithm Using Voxelized Marching Spheres," *Journal of Computational Physics* Vol. 241, 2013, pp. 76-94. doi: 10.1016/j.jcp.2013.01.035

[58] Farhat, C., Lesoinne, M., and LeTallec, P. "Load and Motion Transfer Algorithms for Fluid/Structure Interaction Problems with Non-Matching Discrete Interfaces:Momentum and Energy Conservation, Optimal Discretization and Application to Aeroelasticity," *Computational methods in applied mechanics and engineering* Vol. 157, No. 1-2, 1998.

[59] Donea, J., Huerta, A., and Ponthot, J. *Encyclopedia of Computational Mechanics*, 2004.

[60] Thomas, P. D., and Lombard, C. K. "Geometric Consevation Law and Its Application to Flow Computations on Moving Grids," *AIAA Journal* Vol. 17, No. 10, 1970, pp. 1030-1037. doi: 10.2514/3.61273

[61] Yang, Z., and Mavriplis, D. J. "A Mesh Deformation Strategy Optimized by the Adjoint Method on Unstructured Meshes," 45th AIAA Aerospace Sciences Meeting and Exhibit, Reno, Nevada, 2007, AIAA 2007-557. doi: 10.2514/6.2007-557

[62] Yang, Z., and Mavriplis, D. J. "Higher-Order Time Integration Schemes for Aeroelastic Applications on Unstructured Meshes," *AIAA Journal* Vol. 45, No. 1, 2007, pp. 138-150. doi: 10.2514/1.22847

[63] Mavriplis, D. J., Yang, Z., and Anderson, E. "Adjoint Based Optimization of a Slotted Natural Laminar Flow Wing for Ultra Efficient Flight," AIAA SciTech 2020 Forum, Orlando, Florida, 2020, AIAA 2020-1292. doi: 10.2514/6.2020-1292

[64] Mishra, A., Mavriplis, D. J., and Sitraman, J. "Time-Depedent Aero-Elastic Adjoint-Based Aerodynamic Shape Optimization of Helicopter Rotors in Forward Flight," *AIAA Journal* Vol. 54, No. 12, 2016, pp. 3813-3827. doi: 10.2514/1.J054962

[65] Mani, K."Application of Discrete Adjoint Method to Coupled Multidisciplinary Unsteady Flow Problems for Error Estimation and Optimization," Doctor of Philosophy, Department of Mechanical Engineering, University of Wyoming, Laramie, Wyoming, 2009.

[66] Thornton, E., A., and Dechaumphai , P. "Coupled Flow, Thermal, and Structural Analysis of Aerodynamically Heated Panels," *Journal of aircraft* Vol. 25, No. 11, 1988. doi: 10.2514/3.45702

[67] Thornton, E., and Dechaumphai, P. "Finite Element Prediction of Aerothermal-Structural Interaction of Aerodynamically Heated Panels," AIAA 22nd Thermophysics Conference, Honolulu, Hawaii, 1987, AIAA 87-1610. doi: 10.2514/6.1987-1610

[68] Newman, C., James III, Anderson, W. K., and Whitfield, D. L."Multidisciplinary Sensitivity Derivatives Using Complex Variables," Computational Fluid Dynamics Laboratory, Mississippi State University, Mississipi, USA, 1998.

[69] Gill, P. E., Murray, W., and Saunders, M. A. "SNOPT: An SQP Algorithm for Large-Scale Constrained Optimization," *SIAM review* Vol. 47, No. 1, 2005, pp. 99-131. doi: 10.1137/S0036144504446096